

Use of remote sensing technology in the assessment of resistance of maize to tar spot complex

F. A. Rodrigues Jr.^{1†}, P. Defourny², B. Gérard¹, F. San Vicente¹ and A. Loladze¹

¹International Maize and Wheat Improvement Center – CIMMYT, Mexico; ²Earth and Life Institute, Université Catholique de Louvain, Belgium

Assessment of Tar Spot Complex (TSC) severity in maize breeding experiments is conducted visually and may sometimes result in inconsistencies due to human interpretation. Disease scoring using remote sensing technologies may help bring more precision to the phenotyping process. An experiment for assessment of grain yield losses due to TSC was conducted at the Aguafría Experimental Station of the International Center for Wheat and Maize Improvement – CIMMYT in Mexico. Twenty-five maize genotypes were planted in spring of 2016 under a fungicide treatment to control TSC development and no fungicide treatment in a square lattice design with three replications. Four flights were carried out using an Unmanned Aerial Vehicle (UAV) equipped with a multispectral (550, 660, 735, 790 nm) and a thermal camera, simultaneously with the visual disease scorings and the yield was measured after harvesting. The preliminary results of the study indicated that the use of remote sensing in disease resistance phenotyping may be as effective as visual disease scoring since both correlate highly with the grain yield. Structural and chlorophyll vegetation indices (VIs) proved to be a good alternative for the estimation of yield losses caused by TSC in experimental field conditions, which may be potentially used for screening for resistance to this disease in maize genotypes, hypothetically reducing the need for visual disease scoring in the field.

Keywords: multispectral images, genotype selection, imagery data extraction

Introduction

Tar Spot Complex of Maize (TSC) is one of the major foliar fungal diseases of maize in tropical and sub-tropical environments of some parts of Latin America, mainly in places with higher humidity and moderate climates. The grain loss due to the TSC disease ranges from 50 to 75% depending on the susceptibility of the host and favorable environmental conditions (Hock *et al.*, 1989; Pereyda-Hernández *et al.*, 2009). Three different fungal pathogens are involved in the disease complex: *Phyllachora maydis*, *Monographella maydis* and *Coniothyrium phyllachorae* (Hock *et al.*, 1992). It is believed that *P. maydis* and *M. maydis* play the most important part in the complex causing the maximum damage to the host (Hock *et al.*, 1995).

Resistance to TSC is an important trait that is incorporated to most of the maize lines and hybrids developed by CIMMYT for lowland tropical areas of Latin America. Selection for TSC resistance starts at early generations of breeding population by eliminating susceptible plants. Later on, more advanced generations of the maize lines and hybrids are screened for disease resistance in trials in multiple locations for several years.

The first symptoms of the disease appear as dark spots (stromas) of *P. maydis* on the leaf surface (both lower and upper leaves) usually 2–3 weeks before flowering and the

pustules gradually increase in numbers and size. Approximately two weeks later, the area surrounding the dark spots becomes chlorotic due to the development of the second parasite, *M. maydis*, and develop into the typical “fish eye” symptoms. Usually the chlorotic spots are round or oval in shape but if the disease is developing aggressively the chlorotic circles coalesce and the entire leaves become necrotic, thus affecting the photosynthetic activity and reducing the grain yields.

The phenotyping for TSC resistance is performed on a 1 to 5 scale where 1 represents a completely resistant reaction and 5 is a completely susceptible reaction. The evaluation is done in the field, in adult plants, usually at or just after flowering by visually observing the diseased plots and recording the disease score. This is repeated three to five times during the growing season depending on the disease development. Often the notes, for the severity of the disease are recorded by different personnel causing discrepancies in the disease severity score notes. In addition, preliminary field phenotyping trials are often very large and are time consuming for disease note taking.

Light interception on the leaf surface is differentially absorbed, transmitted or reflected by the leaf depending on its internal structure, chemical composition or physiological status. Spectral imaging sensors detect electromagnetic waves including those not visible to the human eye such as infrared radiation. These data can be combined to identify specific plant features that may not be evident in the visible

† Email: F.A.Rodrigues@cgiar.org

spectrum. Measuring spectral reflectance can thus be used to inform on the health status of the whole plant or to quantify disease infected areas of the plant (Simko *et al.*, 2016).

Laboratory-based spectroscopy technologies have been used to detect different kind of diseases in different crops (Bauriegel and Herppich, 2014; Bauriegel *et al.*, 2011a, 2011b; Bergsträsser *et al.*, 2015). Remote sensing aspects, multi-spectral and hyperspectral imagery had been previously used for disease phenotyping in different crops, such as powdery mildew and leaf rust on wheat (Franke and Menz, 2007), Cercospora leaf spot, sugar beet rust and powdery mildew on sugar beet (Mahlein *et al.*, 2012), huanglongbing disease in orange trees (Garcia-Ruiz *et al.*, 2013) and cotton root rot in cotton (Yang *et al.*, 2010). However, to our knowledge, no such study has been conducted regarding phenotyping TSC on maize. Therefore, the current study was designed to explore how multispectral and thermal images taken from an unmanned aerial vehicle (UAV) may be used to phenotype maize genotypes for TSC resistance, by analyzing the phenotypic and genetic correlations among grain yield, disease scorings and the imaging data. If successful, the study may also help with minimizing the chances of human error in disease phenotyping and potentially reduce the workload in preliminary field trials.

Material and Methods

Field site and data collection

The experiment was conducted at the Aguafría Experimental Station of the International Center for Wheat and Maize Improvement – CIMMYT in Mexico. The experiment was planted in a square lattice design consisting of 25 maize

genotypes in two main blocks, one under fungicide treatment to control TSC development (figures and tables coded as 714) and the second without the treatment (figure and tables coded as 715) in the spring of 2016. Each block contained three randomized replications. Each experimental plot consisted of four 4.5 m length rows with 0.75 m inter-row and 0.25 m plant spacing within row.

The flight campaign were carried out using a fixed wings eBee UAV from SenseFly, equipped with multispectral MultiSpec 4C (550, 660, 735, 790 nm) and ThermoMAP thermal cameras from Arinov, flying at 55 m above ground, yielding a ground resolution of 6 and 12 cm, respectively. Radiometric calibrations were performed before each flight using the standard panel of the multispectral camera provided by the manufacturer. The first disease scoring and a flight were performed simultaneously at the flowering stage (79 days after planting) and a total of four flights and scorings have been conducted at ten-day intervals.

Images were properly geotagged for orthomosaic process using Pix4D mapper®. Later, 10 different vegetation indices (NDVI, RDVI, OSAVI, MSR, MCARI1 and MCARI2 – structural indices; TVI, GM1, PSSRa - chlorophyll indices; G – RGB ratio) were calculated for each image using the necessary wavelengths from the multispectral signal (Rouse *et al.*, 1974; Rougean and Breon, 1995; Rondeaux *et al.*, 1996; Chen, 1996; Haboudane *et al.*, 2004; Broge and Leblanck, 2000; Gitelson and Merzlyak, 1997; Blackburn, 1998; Zarco-Tejada *et al.*, 2005).

Two approaches for image data extractions were tested: (1) average of all pixels contained in a single polygon of both central rows and (2) average of all pixels contained in double polygons, one for each central row (Fig 1).



Figure 1 Zooming of the data extraction approaches: single polygon of both central rows (1), and double polygons, one for each central row (2).

Data analysis

The results of the two different image data extraction approaches were compared by the Pearson’s correlation coefficient using all available information. The phenotypic data were adjusted with respect to the experimental design terms using the restricted maximum likelihood method and the genotypes’ least square means (genotypic) were estimated. The effects of trials, days after sowing and genotypes were considered as fixed, while replication and blocks within replication were considered as random effects. Thus, both phenotypic and genotypic data were used for individual association by means of the Pearson’s correlation coefficients among grain yield, diseases scorings and vegetation indices in each treatment and each survey date (79, 90, 100 and 113 days after sowing). All analyses were performed with the R software and lme4 and lsmeans packages.

Results and discussion

The comparison between both data extraction approaches is presented in Figure 2. Although it was expected that approach 2 (double polygons, Figure 1) would be more accurate since it did not carry the furrow data reflectance, both approaches

yielded similar results, with the coefficient of correlation of all VIs, wavelengths and canopy temperature close to 1 (Figure 2). Based on these results, it had been decided to use only the data extracted with approach 2 for the following data analysis.

The correlation of the yield phenotypic and genotypic data with VIs, thermal information and disease scoring (TS) are shown in Tables 1 and 2, respectively. The phenotypic correlations demonstrated how the secondary data (images and TS) were related to yield variation in the field without taking into account the genotypic effects, while the genotypic correlations were analyzed based on the least square means of the grain yield, which took into account the effect of the genotype on yield.

The majority of the image variables showed different degrees of phenotypic correlation with yield in the fields with and without the fungicide treatment, although some variables were not significant ($p > 0.1$). TS showed non-significant correlations with the fungicide treatment since the disease development was controlled. The highest coefficient of TS across the dates was -0.43 in the non-fungicide treatment, which was lower than the correlations of the VIs of the corresponding images. The correlation of the VIs with

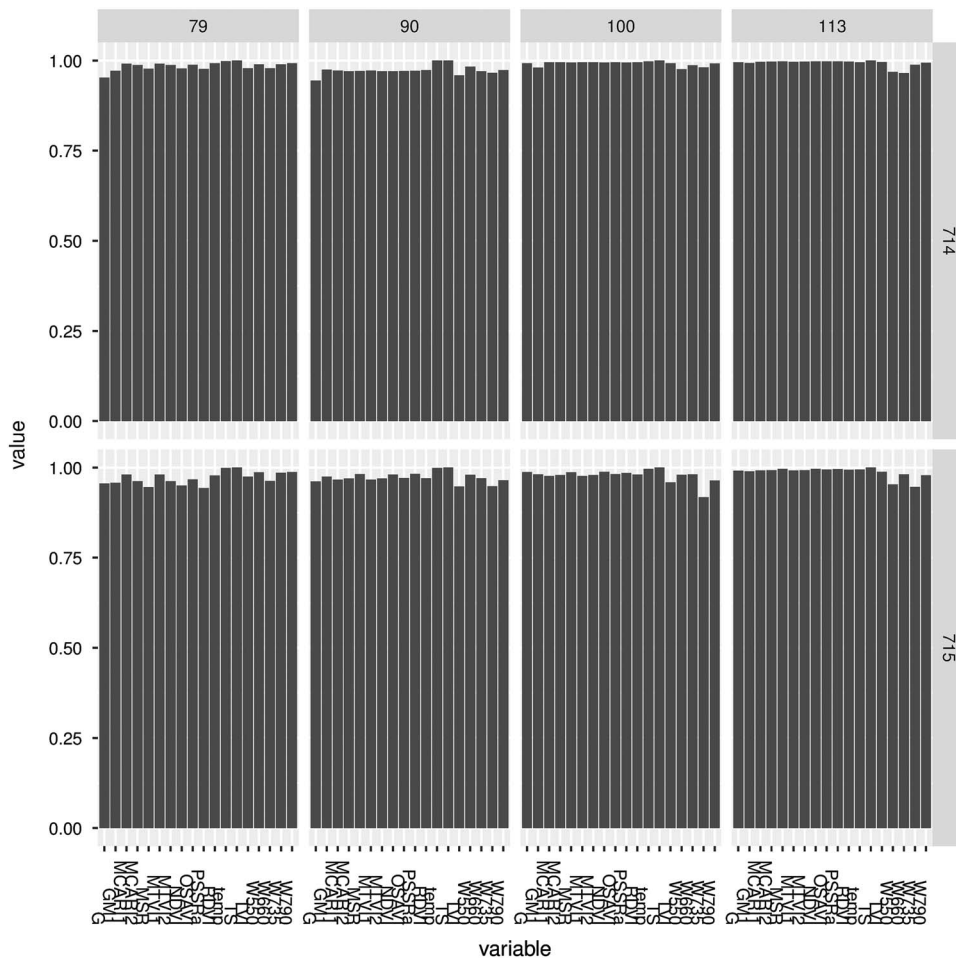


Figure 2 Coefficient of correlation between both data extraction approaches for VIs, wavelengths and canopy temperature. Where: NDVI, RDVI, OSaVI, MSR, MCARI1 and MCARI2 – structural indices; TVI, GM1, PSSRa – chlorophyll indices; G – RGB ratio; TS – visual disease scoring; temp – canopy temperature; W550, W660, W735, W790 – reflectance wavelengths (nm); 714 – fungicide treatment; 715 – Non-fungicide treatment.

Table 1 Phenotypic correlation between yield, image data and visual scoring (n = 75).

| | 714 | | | | 715 | | | |
|---------|--------|-------|--------|-------|--------|---------|--------|--------|
| | 79 | 90 | 100 | 113 | 79 | 90 | 100 | 113 |
| NDVI | 0.31* | 0.31* | 0.47* | 0.54* | 0.42* | 0.51* | 0.63* | 0.57* |
| RDVI | 0.28* | 0.36* | 0.51* | 0.55* | 0.55* | 0.59* | 0.67* | 0.59* |
| OSAVI | 0.31* | 0.36* | 0.50* | 0.55* | 0.55* | 0.58* | 0.66* | 0.59* |
| MSR | 0.30* | 0.31* | 0.49* | 0.56* | 0.42* | 0.52* | 0.68* | 0.58* |
| MCARI1 | 0.22** | 0.35* | 0.47* | 0.53* | 0.51* | 0.60* | 0.65* | 0.58* |
| MCARI2 | 0.29* | 0.35* | 0.48* | 0.54* | 0.57* | 0.60* | 0.66* | 0.58* |
| TVI | -0.09 | 0.27* | 0.25** | 0.42* | 0.15 | 0.58* | 0.57* | 0.53* |
| GM1 | 0.11 | 0.36* | 0.39* | 0.48* | 0.23** | 0.49* | 0.64* | 0.60* |
| PSSRa | 0.29* | 0.31* | 0.50* | 0.58* | 0.42* | 0.53* | 0.72* | 0.61* |
| G | -0.02 | 0.05 | 0.12 | 0.34* | 0.12 | 0.38* | 0.52* | 0.51* |
| Thermal | -0.12 | 0.35* | -0.36* | 0.19 | -0.13 | 0.01 | -0.46* | 0.00 |
| TS | 0.08 | -0.01 | -0.05 | -0.07 | -0.30* | -0.24** | -0.39* | -0.43* |

Where: NDVI, RDVI, OSAVI, MSR, MCARI1 and MCARI2 – structural indices; TVI, GM1, PSSRa – chlorophyll indices; G – RGB ratio; thermal – canopy temperature; TS – visual disease scoring; 714 – fungicide treatment; 715 – Non-fungicide treatment. 79, 90, 100 and 113 days after sowing. * Coefficients of correlation statistically significant at 1% probability; ** coefficients of correlation statistically significant at 5% probability.

Table 2 Genetic correlation between yield, image data and visual scoring (n = 25).

| | 714 | | | | 715 | | | |
|---------|----------|---------|---------|---------|--------|---------|--------|--------|
| | 79 | 90 | 100 | 113 | 79 | 90 | 100 | 113 |
| NDVI | 0.29 | 0.21 | 0.40** | 0.45** | 0.09 | 0.26 | 0.58* | 0.54* |
| RDVI | 0.56* | 0.38*** | 0.44** | 0.45** | 0.53* | 0.48* | 0.60* | 0.55* |
| OSAVI | 0.50* | 0.34*** | 0.43** | 0.45** | 0.52* | 0.45** | 0.60* | 0.55* |
| MSR | 0.26 | 0.22 | 0.39*** | 0.46** | 0.09 | 0.30 | 0.62* | 0.54* |
| MCARI1 | 0.56* | 0.46** | 0.43** | 0.43** | 0.51* | 0.52* | 0.60* | 0.54* |
| MCARI2 | 0.55* | 0.39** | 0.43** | 0.43** | 0.57* | 0.51* | 0.61* | 0.55* |
| TVI | 0.36*** | 0.44** | 0.36*** | 0.39** | 0.42** | 0.54* | 0.57* | 0.54* |
| GM1 | 0.00 | 0.19 | 0.23 | 0.38*** | -0.25 | 0.13 | 0.52* | 0.53* |
| PSSRa | 0.24 | 0.22 | 0.38*** | 0.46** | 0.09 | 0.32 | 0.65* | 0.55* |
| G | 0.24 | 0.24 | 0.32 | 0.37*** | 0.26 | 0.38*** | 0.60* | 0.54* |
| Thermal | -0.36*** | 0.56* | -0.50* | -0.27 | -0.17 | -0.10 | -0.57* | -0.33* |
| TS | -0.19 | -0.10 | -0.11 | -0.14 | -0.61* | -0.51* | -0.62* | -0.60* |

Where: NDVI, RDVI, OSAVI, MSR, MCARI1 and MCARI2 – structural indices; TVI, GM1, PSSRa – chlorophyll indices; G – RGB ratio; thermal – canopy temperature; TS – visual disease scoring; 714 – fungicide treatment; 715 – Non-fungicide treatment. 79, 90, 100 and 113 days after sowing. * Coefficients of correlation statistically significant at 1% probability; ** coefficients of correlation statistically significant at 5% probability; *** coefficients of correlation statistically significant at 10% probability.

the yield under the fungicide treatment was slightly higher ($p < 0.01$) with the images acquired from the last flight performed at 113 days after sowing (das). Furthermore, under the non-fungicide treatment the disease scores had lower coefficients than the majority of VIs correlations of the whole flight campaign, being considerably lower in comparison with VIs correlations at with the second flight (90 das; TS = -0.24).

As in case of the phenotypic correlation, no significant genotypic correlation between TS and yield under the fungicide treatment was observed due to the absence of the disease that would have resulted in the reduction of the grain yield. However, correlations have been observed between the VIs, thermal indices and yield. Even though the disease scores showed slightly higher genotypic correlations than the VIs under no fungicide treatment just at the first and last

images (-0.61 and -0.60, respectively), the maximum difference of the correlation coefficients reached only 5 units. The correlations of the structural and chlorophyll VIs were higher than and/or equal to TS at the second and the third dates of the flight campaign (90 and 100 das, respectively). The structural and chlorophyll indices, such as MSR and PSSRa, had the highest coefficients among all of the remote sensing variables (0.62 and 0.65, respectively) from the image obtained at 100 das. In other previous studies it was demonstrated that NDVI – which is a structural index, had moderate to high accuracy on distinguishing levels of resistance of wheat infected with leaf rust (Franke and Menz, 2007) and Sunn pest (Genc *et al.*, 2008).

These preliminary results showing the potential of the remote sensing approach is the first step for developing high throughput phenotyping methods for TSC resistance in

maize. Furthermore, the combination of different VIs into multivariate models and machine learning procedures will need to be explored further targeting early detection of the reduction of photosynthetic activities caused by TSC. This could also open further possibilities to develop techniques for upscaling the use of remote sensing in estimating damages caused by TSC in the farmers' fields, providing information for timely crop management.

Conclusions

Structural and chlorophyll VIs proved to be a promising tool for the estimation of yield losses caused by TSC and offering new opportunities for high throughput phenotyping for resistance of maize to this highly important foliar disease. The experiment will be repeated in the next maize growing cycle to account for possible environmental variability and to ensure the repeatability of the methodology. Also different imagery data extraction methods will be tested to optimize the phenotyping effectiveness and precision while minimizing the possibilities of errors occurring during the process.

Acknowledgements

We would like to thank the Maize CGIAR Research Program (Maize CRP) for providing funds for the study. We are thankful to Mr. Carlos Muñoz for his technical assistance in the field, Ms. Lorena González Pérez for her assistance with the image processing and the Biometric and Statistics Unit of CIMMYT for their support on the data analysis.

References

- Bauriegel E, Giebel A, Geyer M, Schmidt U and Herpich W 2011b. Early detection of Fusarium infection in wheat using hyper-spectral imaging. *Computer Electronics Agriculture* 75, 304–312.
- Bauriegel E, Giebel A and Herpich WB 2011a. Hyperspectral and chlorophyll fluorescence imaging to analyze the impact of Fusarium culmorum on the photosynthetic integrity of infected wheat ears. *Sensors (Basel Switzerland)* 11, 3765–3779.
- Bauriegel E and Herpich WB 2014. Hyperspectral and chlorophyll fluorescence imaging for early detection of plant diseases, with special reference to Fusarium spec. infections on wheat. *Agriculture* 4, 32–57.
- Bergsträsser S, Fanourakis D, Schmittgen S, Cendrero-Mateo MP, Jansen M, Scharr H and Rascher U 2015. HyperART: Non-invasive quantification of leaf traits using hyperspectral absorption-reflectance-transmittance imaging. *Plant Methods* 11, 1–17.
- Blackburn GA 1998. Spectral indices for estimating photosynthetic pigment concentrations: a test using senescent tree leaves. *International Journal of Remote Sensing* 19, 657–675.
- Broge NH and Leblanc E 2000. Comparing prediction power and stability of broadband and hyperspectral vegetation indices for estimation of green leaf area index and canopy chlorophyll density. *Remote Sensing of Environment* 76, 156–172.
- Chen J 1996. Evaluation of vegetation indices and modified simple ratio for boreal applications. *Canadian Journal of Remote Sensing* 22, 229–242.
- Franke J and Menz G 2007. Multi-temporal wheat disease detection by multi-spectral remote sensing. *Precision Agriculture* 8, 161–172.
- García-Ruiz F, Sankaran S, Maja JM, Lee WS, Rasmussen J and Ehsani R 2013. Comparison of two aerial imaging platforms for identification of Huanglongbing-infected citrus trees. *Computer Electronics Agriculture* 91, 106–115.
- Genc H, Genc L, Turhan H, Smith S and Nation 2008. Vegetation indices as indicators of damage by the sunn pest (Hemiptera: Scutelleridae) to field grown wheat. *African Journal of Biotechnology* 7, 173–180.
- Gitelson AA and Merzlyak MN 1997. Remote estimation of chlorophyll content in higher plant leaves. *International Journal of Remote Sensing* 18, 2691–2697.
- Haboudane D, Miller JR, Pattey E, Zarco-Tejada PJ and Stra-Chan I 2004. Hyperspectral vegetation indices and novel algorithms for predicting green LAI of crop canopies: Modeling and validation in the context of precision agriculture. *Remote Sensing of Environment* 90, 337–352.
- Hock J, Krans J and Renfro BL 1989. El 'complejo "mancha de asfalto" del maíz, su distribución geográfica, requisitos ambientales e importancia económica en México. *Revista Mexicana de Fitopatología* 7, 129–135.
- Hock J, Kranz J and Renfro BL 1992. Tests of standard diagrams for field use in assessing the tar spot disease complex of maize (*Zea mays*). *Tropical Pest Management* 38 (3), 314–318.
- Hock J, Kranz J and Renfro BL 1995. Studies on the epidemiology of the tar spot disease complex of maize in Mexico. *Plant Pathology* 44, 490–502.
- Mahlein AK, Steiner U, Hillnhütter C, Dehne HW and Oerke EC 2012. Hyperspectral imaging for small-scale analysis of symptoms caused by different sugar beet disease. *Plant methods* 2012, 8 (3).
- Pereyda-Hernández J, Hernández-Morales J, Sandoval-Islas S, Aranda-Ocampo S, de León C and Gómez-Montiel N 2009. Etiología y manejo de la mancha de asfalto (*Phyllachora maydis* Maubl.) del maíz en Guerrero, México. *Agrociencia* 43 (5), 511–519.
- Rondeaux G, Steven M and Baret F 1996. Optimization of soil adjusted vegetation indices. *Remote Sensing of Environment* 55, 95–107.
- Rougean JL and Breon FM 1995. Estimating PAR absorbed by vegetation from bidirectional reflectance measurements. *Remote Sensing of Environment* 51, 375–384.
- Rouse JW, Haas RH, Schell JA, Deering DW and Harlan JC 1974. Monitoring the vernal advancements and retrogradation of natural vegetation. NASA/GSFC, Greenbelt, MD.
- Simko I, Jimenez-Berni JA and Sirault XRR 2016. Phenomic approaches and tools for phytopathologists. *Phytopathology* 107 (1), 6–17.
- Yang C, Everitt JH and Fernandez CJ 2010. Comparison of airborne multispectral and hyperspectral imagery for mapping cotton root rot. *Biosystem Engineering* 107, 131–139.
- Zarco-Tejada PJ, Berjón A, López-Lozano R, Miller JR, Marin P, Cachorro V, Gonzales MR and de Fruto A 2005. Assessing vineyard condition with hyperspectral indices: Leaf and canopy reflectance simulation in a row-structured discontinuous canopy. *Remote Sensing of Environment* 99, 271–287.